

INSIGHT: Enhancing Autonomous Driving Safety through Vision-Language Models on Context-Aware Hazard Detection and Edge Case Evaluation

Dianwei Chen ^{*}, Zifan Zhang [†], Yuchen Liu [†], Xianfeng Terry Yang ^{*}

Abstract—Autonomous driving systems face significant challenges in handling unpredictable edge-case scenarios, such as adversarial pedestrian movements, dangerous vehicle maneuvers, and sudden environmental changes. Current end-to-end driving models struggle with generalization to these rare events due to limitations in traditional detection and prediction approaches. To address this, we propose INSIGHT (Integration of Semantic and Visual Inputs for Generalized Hazard Tracking), a hierarchical vision-language model (VLM) framework designed to enhance hazard detection and edge-case evaluation. By using multimodal data fusion, our approach integrates semantic and visual representations, enabling precise interpretation of driving scenarios and accurate forecasting of potential dangers. Through supervised fine-tuning of VLMs, we optimize spatial hazard localization using attention-based mechanisms and coordinate regression techniques. Experimental results on the BDD100K dataset demonstrate a substantial improvement in hazard prediction straightforwardness and accuracy over existing models, achieving a notable increase in generalization performance. This advancement enhances the robustness and safety of autonomous driving systems, ensuring improved situational awareness and potential decision-making in complex real-world scenarios.

Index Terms—Vision-language model, autonomous driving, edge driving cases, hazard detection

I. INTRODUCTION

In autonomous driving scenarios, there exists a possibility that unpredictable edge cases, such as pedestrian crossing and construction zones, will occur in the next time steps [1]. These unforeseen edge cases can lead to dangerous consequences, including vehicle crashes, pedestrian injuries, etc. Therefore, it is necessary to develop a precise and generalized model to interpret the current driving scenario and draw out unpredictable dangerous scenarios. By connecting end-to-end and prediction models, autonomous vehicles are able to prevent effects from possible dangerous edge cases with advanced autonomous driving algorithms [2].

However, connecting current autonomous driving models and edge cases prediction models is challenging [1]. The traditional detection algorithms, such as the sensor-based autonomous driving model [3], do not perform well on edge

cases due to the lack of explicit expression of any semantic concepts. The vision-language model (VLM) is a useful tool for developing high-hierarchy auxiliary algorithms. It is built by integrating a large language model (LLM) and a vision encoder, which can take joint visual and textual input and generate textual responses. The vision-language adapter architecture enables collaborative understandings of multimodal datasets, such as video, image, and natural language. With the ability of generalization and extraction from higher-level semantic information, the VLMs can utilize the pretrained knowledge, support the natural language commands, and deal with various, complicated, and even unseen driving scenarios [4], [5].

In this paper, we introduce a novel framework, namely INSIGHT (Integration of Semantic and Visual Inputs for Generalized Hazard Tracking). With the connection of visual and textual inputs, the model can draw a precise description of the current scenario and forecast the dangerous location for future scenarios. It provides sufficient generalization ability when facing unexpected pedestrian and vehicle behaviors or sudden surrounding changes (e.g., emergency vehicles or debris on the road). The model is trained by using a multi-modal approach, extracting visual features with a Vision Transformer and fusing them with text embeddings from a pre-trained language model. It is also fine-tuned on an annotated dataset to optimize potential hazard edge case detection. Our contribution is summarized in three folds:

- Utilize the vision-language model to combine semantic and visual inputs to enhance hazard detection and improve generalization ability in edge cases.
- Achieve the goal of precise location detection by using an attention map localization for loss function of supervised fine-tuning VLMs.
- Simulation studies show that INSIGHT effectively focuses on detecting potential hazard edge case areas that baseline and traditional models cannot complete.

II. RELATED WORKS

Recently, the development of autonomous driving algorithms has significantly improved with various approaches addressing scene understanding, prediction, and control [6]–[8]. This section reviews relevant work in edge case scenario exploration, end-to-end autonomous driving models, and VLMs in autonomous vehicles.

This work is supported NDSU VPR Office project, Accelerating the Deployment of Autonomous Vehicles in Rural Areas, and National Science Foundation under Award SaTC–2350075.

^{*} D. Chen and XT. Yang are with the College of Engineering, University of Maryland, College Park, MD 20742, USA. (Email: {dwchen98, xtyang}@umd.edu). (Corresponding author: Xianfeng Terry Yang.)

[†] Z. Zhang and Y. Liu are with the Department of Computer Science, North Carolina State University, Raleigh, NC, 27695, USA (Email: {zzhang66, yuchen.liu}@ncsu.edu).

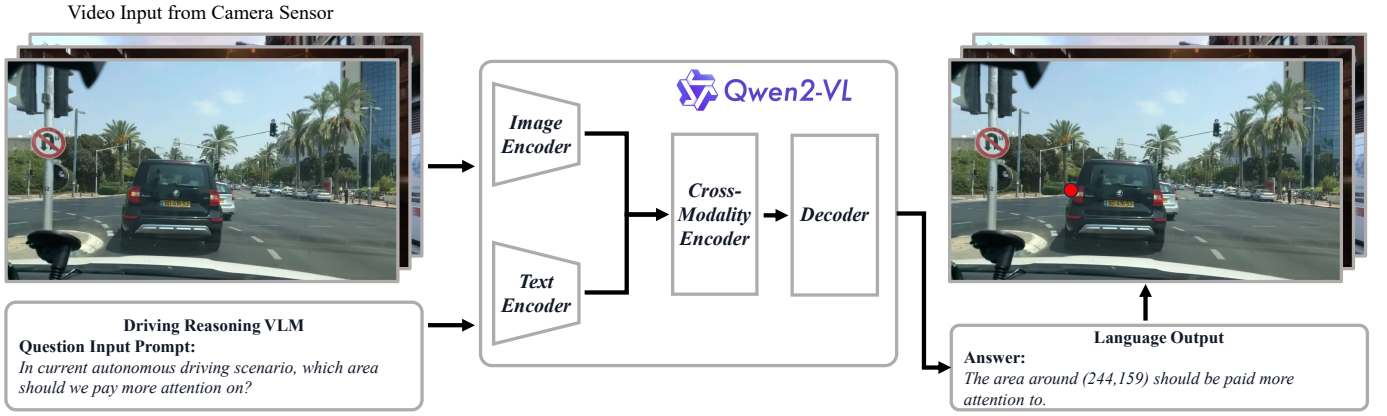


Fig. 1: Integration of Semantic and Visual Inputs for Generalized Hazard Tracking through Supervised Fine-tuning VLMs

A. Edge Case Scenario Exploration

Edge case scenarios in autonomous driving refer to rare, unpredictable, or extreme situations that challenge the robustness and safety of autonomous driving algorithms [9], [10]. Verifying both the vehicle and its algorithms in these edge cases is critical to ensuring safety and reliability [1]. Testing in such scenarios involves subjecting the vehicle and its systems to high-risk or failure-prone conditions, allowing for a comprehensive evaluation of their performance under adverse circumstances [11], [12]. These simulations play a vital role in rigorously testing and refining algorithms and vehicle systems, enabling the identification and resolution of potential weaknesses [13]. After verifying and even training in such scenarios, these vehicles are able to not only enhance the robustness of autonomous systems but also accelerate their deployment in real-world settings by ensuring they meet safety and performance standards under a wide range of conditions. Extensive research has been conducted to model and simulate edge case scenarios, focusing on conditions such as extreme weather, erratic pedestrian behavior, and unconventional vehicle movements [14]–[17]. By addressing these issues in simulated environments, developers can ensure a higher level of safety and performance before deploying the systems in real-world applications [18]. This proactive approach is essential for building trust in autonomous driving technologies and mitigating risks associated with edge cases.

B. End-to-End Autonomous Driving Model

End-to-end models for autonomous driving utilize deep learning architectures to map raw sensor inputs, such as images and LiDAR data, directly to control outputs like steering, acceleration, and braking. Convolutional neural network (CNN) is a common model employed to process visual data by extracting spatial features from camera inputs, enabling the recognition of lanes, vehicles, and other road elements [19], [20]. Recurrent neural network (RNN) and temporal convolutional network (TCN) handle data sequences effectively, capturing dynamic changes in the environment over time [21]. Moreover, transformer utilizes self-attention mechanisms to

effectively model long-range dependencies and complex interactions for both visual and sequential data processing [22], [23], offering improved performance in tasks such as object detection, trajectory prediction, and scene understanding [24]. While effective in many scenarios, these models often face challenges in rare or hard-to-predict edge cases due to their reliance on the data used during training, which is collected from daily common driving scenarios or simple AV simulator scenarios [25], which may not fully represent real-world variability.

C. Vision-Language Model in Autonomous Vehicle

In recent years, VLM has made breakthroughs in natural language processing and multimodal tasks [4], [26]. Applying it to autonomous driving can effectively improve scene understanding and decision-making capabilities [5], [27]. VLMs enhance the system’s comprehensive perception capabilities by combining visual data, such as cameras and LiDAR, and textual data, such as traffic signs and navigation instructions [28]–[30]. The effective integration of visual features and language representation through visual language adapters can improve the ability to understand complex driving scenarios [31]. With large-scale pre-trained VLMs, the model can learn common representations and knowledge from massive multi-modal data, assisted with zero-shot learning [32], [33], thus having strong generalization capabilities [34], [35]. The model can infer semantic information such as the meaning of the potential movement of a pulled-over vehicle with law enforcement on the side from visual features in an image [36]. This ability allows the model to use pre-trained knowledge to make inferences about unknown data when encountering new scenarios, without relying on task-specific annotated data [37]. In our work, we use VLM to unify visual and language understanding in autonomous driving, enabling real-time decisions, better scene comprehension, and improved edge case handling for safer and more efficient driving automation.

III. METHOD

Our proposed method consists of four main components: modal feature extraction, shared latent space projection, se-

Algorithm 1 INSIGHT: Fine-Tuning for Integration of Semantic and Visual Inputs for Generalized Hazard Tracking

- 1: **Input:** Pre-trained model M_0 , dataset D , learning rate η , epochs E , batch size B , coefficients $\lambda_{\text{coord}}, \lambda_{\text{text}}$
- 2: Initialize model with LoRA-adapted projection layers
- 3: Tokenize D and split into D_{train} and D_{val}
- 4: Define loss function:

$$L_{\text{total}} = \lambda_{\text{coord}} L_{\text{coord}} + \lambda_{\text{text}} L_{\text{text}}$$

- 5: **for** $e = 1$ **to** E **do**
- 6: **for** batch B_b in D_{train} **do**
- 7: Extract vision and text embeddings
- 8: Output attention coordinates (\hat{x}, \hat{y})
- 9: Generate descriptive text \hat{s}_{text}
- 10: Compute losses:

$$L_{\text{coord}} = \frac{1}{N} \sum_{i=1}^N \|\hat{loc}_i - loc_i\|^2$$

$$L_{\text{text}} = -\frac{1}{N} \sum_{i=1}^N \sum_{t=1}^T s_{i,t} \log(\hat{s}_{i,t})$$

$$L_{\text{total}} = \lambda_{\text{coord}} L_{\text{coord}} + \lambda_{\text{text}} L_{\text{text}}$$

- 11: Update model parameters via gradient descent
 - 12: **end for**
 - 13: Evaluate M on D_{val}
 - 14: **end for**
 - 15: **Output:** Fine-tuned model M_{sft}
-

mantic alignment, and hazard region localization. It includes extracting key features from visual and textual data for multimodal processing, mapping features into a unified space for seamless modality interaction, aligning visual and textual data for contextual understanding, and identifying and locating potential hazards in the driving environment.

A. Modal Feature Extraction

Qwen2-VL uses a transformer-based architecture with special encoders for visual and textual data:

- **Vision Encoder:** The Vision Transformer (ViT) divides input images into non-overlapping patches and extracts features for each patch. It captures spatial and structural details from images by analyzing individual patches, enabling a comprehensive understanding of visual inputs.
- **Text Encoder:** A transformer-based model processes tokenized text sequences. It focuses on linguistic context and semantic relationships within tokenized text sequences, ensuring that textual information is accurately represented and aligned with the visual features.

Together, these encoders facilitate robust multimodal reasoning and integration.

B. Supervised Fine-tuning VLMs

C. Shared Latent Space

Both visual and textual features are projected into a shared latent space $V \subseteq \mathbb{R}^k$ through projection layers, enabling cross-modal understanding:

$$E_{\text{img}} = \text{Projector}_{\text{img}}(F_{\text{img}}), \quad E_{\text{text}} = \text{Projector}_{\text{text}}(F_{\text{text}}) \quad (1)$$

The projection layer maps high-dimensional visual and textual features into a shared lower-dimensional latent space using a linear transformation or an MLP. This shared space ensures that visual and textual inputs are comparable and seamlessly fused.

D. Attention Maps for Spatial Localization

Our proposed method employs a transformer-based architecture that generates multimodal embeddings by integrating visual and textual features. To enable spatial localization, we extract attention maps from its vision encoder, which inherently capture the regions of the input image that contribute most to the model's understanding. These attention maps, denoted as $A \in \mathbb{R}^{H \times W}$, represent a spatial distribution of importance over the image, where H and W are the height and width of the feature map.

1) *Extracting Coordinates from Attention Maps:* To localize specific regions of interest, the method will identify the most prominent areas in the attention map. By computing attention weights for each spatial location using the outputs of the last layer of the vision encoder. The spatial coordinates of the maximum attention weight, (\hat{x}, \hat{y}) , are identified as the predicted location of the target:

$$(\hat{x}, \hat{y}) = \arg \max_{(x,y)} A(x, y) \quad (2)$$

2) *Integration with Text Generation:* The extracted coordinates are further integrated with the language generation module to produce descriptive outputs. For instance, the model generates text such as: "The area around (544, 459) should be paid more attention to." by conditioning the language generation layers on the localized regions.

E. Loss Function:

The training process adopts a multi-task loss function to simultaneously optimize coordinate prediction and text generation. The total loss is defined as

$$L_{\text{total}} = \lambda_{\text{coord}} L_{\text{coord}} + \lambda_{\text{text}} L_{\text{text}}, \quad (3)$$

as shown in Algorithm 1 (lines 4, 10), with:

- L_{coord} : Coordinate regression loss, computed as the Mean Squared Error (MSE) between the coordinates extracted from the attention map and the ground-truth coordinates. For each example i , we first obtain

$$(\hat{x}_i, \hat{y}_i) = \arg \max_{(x,y)} A_i(x, y), \quad (4)$$

where $A_i \in \mathbb{R}^{H \times W}$ is the last-layer attention map for image i . Then

$$L_{\text{coord}} = \frac{1}{N} \sum_{i=1}^N \|(\hat{x}_i, \hat{y}_i) - (x_i, y_i)\|^2. \quad (5)$$

- L_{text} : Text generation loss, computed as the cross-entropy between the generated token probabilities and the ground-truth tokens:

$$L_{\text{text}} = -\frac{1}{N} \sum_{i=1}^N \sum_{t=1}^T s_{i,t} \log \hat{s}_{i,t}, \quad (6)$$

where T is the sequence length, $s_{i,t}$ the true token indicator, and $\hat{s}_{i,t}$ the model's predicted probability.

- $\lambda_{\text{coord}}, \lambda_{\text{text}}$: Balancing coefficients that weight the relative importance of the two tasks.

This loss design ensures that the model learns to focus its attention correctly (via L_{coord}) while also producing contextually coherent textual descriptions (via L_{text}).

F. Convergence Derivation and Stability Analysis for AdamW

Now to sketch a convergence argument for our multi-task loss under the AdamW optimizer for the default Huggingface trainer setting, first need to let

$$L_{\text{total}}(\theta) = \lambda_{\text{coord}} L_{\text{coord}}(\theta) + \lambda_{\text{text}} L_{\text{text}}(\theta). \quad (7)$$

Assume:

- 1) **Lower-Boundedness**: $L_{\text{total}}(\theta) \geq 0$ for all θ .
- 2) **L -Smoothness**: Each $L_i(\theta)$ is L -Lipschitz-smooth, so ∇L_{total} is also L -Lipschitz.
- 3) **Bounded Gradients**: There exists $G > 0$ such that $\|\nabla L_{\text{total}}(\theta)\| \leq G$ for all θ .

AdamW maintains per-parameter first and second moment estimates:

$$m_{t+1} = \beta_1 m_t + (1 - \beta_1) g_t, \quad v_{t+1} = \beta_2 v_t + (1 - \beta_2) g_t^2, \quad (8)$$

where $g_t = \nabla L_{\text{total}}(\theta_t)$, and then computes the bias-corrected moments:

$$\hat{m}_{t+1} = \frac{m_{t+1}}{1 - \beta_1^{t+1}}, \quad \hat{v}_{t+1} = \frac{v_{t+1}}{1 - \beta_2^{t+1}}. \quad (9)$$

The parameter update with decoupled weight decay λ is

$$\theta_{t+1} = \theta_t - \eta_t \frac{\hat{m}_{t+1}}{\sqrt{\hat{v}_{t+1}} + \epsilon} - \eta_t \lambda \theta_t. \quad (10)$$

Under the standard conditions on the decaying step sizes

$$\sum_{t=0}^{\infty} \eta_t = \infty, \quad \sum_{t=0}^{\infty} \eta_t^2 < \infty, \quad (11)$$

and choosing β_1, β_2 such that $1 - \beta_1 = O(\eta_t)$, one can invoke the convergence result of [38] to show:

$$\min_{0 \leq t < T} \mathbb{E} \|\nabla L_{\text{total}}(\theta_t)\|^2 = O\left(\frac{1}{\sqrt{T}}\right). \quad (12)$$

In particular, AdamW yields a sublinear convergence rate in expectation:

$$\frac{1}{T} \sum_{t=0}^{T-1} \mathbb{E} \|\nabla L_{\text{total}}(\theta_t)\|^2 \leq \frac{C}{\sqrt{T}}, \quad (13)$$

for some constant C depending on L, G, β_1, β_2 , and the initial parameter norm. Hence as $T \rightarrow \infty$, $\mathbb{E} \|\nabla L_{\text{total}}(\theta_t)\| \rightarrow 0$, i.e. the parameters converge to a stationary point in expectation.

Attention-based localization method removes the need for explicit bounding box annotations, while the multi-task loss ensures end-to-end optimization, making it both efficient and effective for scene understanding compared to a traditional end-to-end black box model.

This methodology, as shown in Fig. 1, enables accurate prediction of potential hazard regions in autonomous driving scenarios by utilizing fine-tuned vision-language alignment, precise localization mechanisms, and a combined focus on coordinate regression and textual explanation.

G. Dataset Preprocessing

1) **Dataset Overview**: The dataset used in this study is a subset of the BDD100K dataset, containing 1000 images selected from front-facing camera recordings in autonomous driving scenarios. These images cover diverse environments, including urban, suburban, and highway scenes, with varying lighting and weather conditions. A custom dataset is created by manually annotating this selective portion of images, where each image is labeled with potential hazard points (x, y) based on human judgment and driving experience (Fig. 2). The annotation criteria focused on identifying areas likely to pose risks, such as pedestrians, vehicles in proximity, or sudden obstacles. The subset of 1000 images is selected to maintain efficiency and reduce computational costs while still enabling effective model evaluation and training on key scenarios.

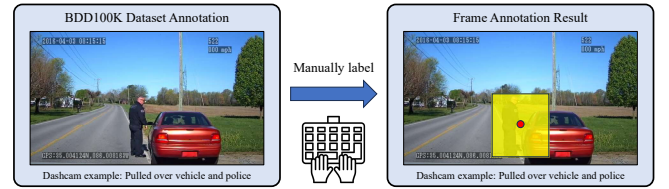
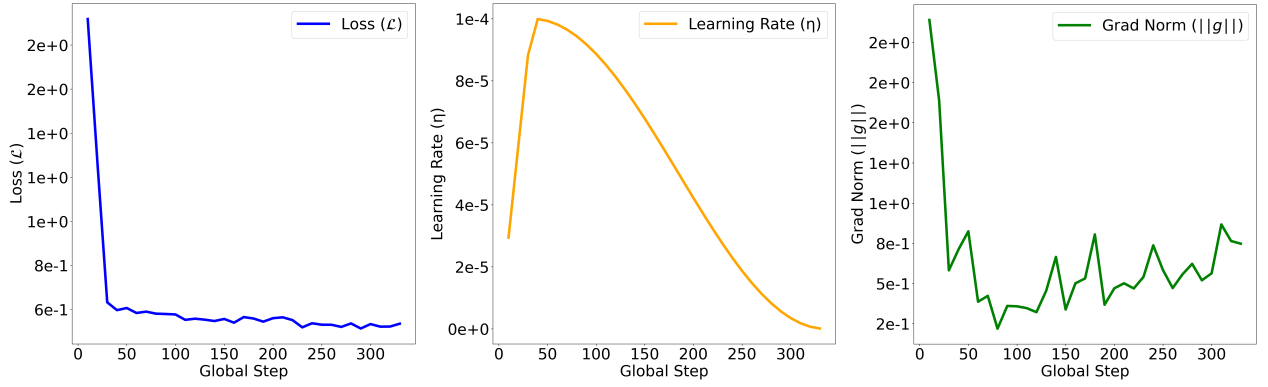


Fig. 2: Manual Annotation for dataset preprocessing

2) **Annotation Method**: Manual annotation is performed to label potential hazard areas within each image. The hazard area is defined based on the experimental subjects' driving experience and judgment, including areas where pedestrians, vehicles, or other obstacles pose potential risks to safe driving. In general, these potential hazard areas can be divided into two categories: predictable surrounding behavior (e.g., a vehicle in an adjacent lane attempting to merge) and unpredictable surrounding behavior (e.g., a pedestrian suddenly stepping onto the road).

For consistency, one experimental subject annotated all 1000 images in this dataset. During this annotation process, each frame is displayed for a maximum of 5 seconds, during which



(a) Training loss of the supervised fine-tuning on Qwen2-VL-7B (b) Learning rate of the supervised fine-tuning on Qwen2-VL-7B (c) Grad norm of the supervised fine-tuning on Qwen2-VL-7B

Fig. 3: Supervised fine-tuning metrics on Qwen2-VL-7B.

the subject identifies the area with the highest probability of collision risk. A bounding box is drawn around the identified hazard area, and its center point is recorded as (x, y) coordinates. Each annotated image contains exactly one identified hazard area. To validate the reliability of these annotations, a subset of 100 images is cross-checked by two additional reviewers; discrepancies are discussed and resolved, resulting in a final consensus annotation for the entire dataset.

H. Model Setup

1) *Pre-trained Model*: Qwen2-VL-7B is chosen as the baseline pre-trained model [39], while it can be easily extended to other pre-trained VLM models. This VLM is designed for multi-modal tasks, combining robust image and text processing capabilities. Also, with the incorporation of the vision transformer for visual encoding and the transformer-based text encoder for language understanding, it's easy to enable the model to handle complex multi-modal tasks effectively. The pre-trained weights are sourced from the HuggingFace library, and the base architecture is kept unchanged during fine-tuning, except for specific layers adapted using LoRA.

2) *Fine-tuning Strategy*: LoRA is employed as a parameter fine-tuning technique to adapt the pre-trained model for hazard region prediction. LoRA is applied to the multi-head attention layers (Query and Value projection matrices in the attention mechanism) and feed-forward layers (Selected layer of the output feed-forward network). The other weights in the pre-trained model remained frozen during training. The Rank r of the LoRA matrices is set to 8. The pre-trained weights $W \in \mathbb{R}^{d \times k}$ are adapted as follows:

$$W' = W + \Delta W, \Delta W = A \cdot B, A \in \mathbb{R}^{d \times r}, B \in \mathbb{R}^{r \times k}, \quad (14)$$

where A and B are learnable matrices, and r is the low rank, significantly reducing the number of trainable parameters.

IV. EXPERIMENTS

A. Hyperparameter Configuration

The AdamW optimizer which includes the weight decaying for regularization is used in the experiment. The initial learning

rate is set to 1×10^{-4} and is decayed based on the cosine schedule as $\eta_t = \eta_0 \cdot 0.5 \left(1 + \cos\left(\frac{t}{T}\pi\right)\right)$, where η_t is learning rate at step t , and T is total number of training steps. Also due to the memory constraints, a single image per batch is processed with gradient accumulation performed over 8 steps before parameter updates. The model is trained for 3 epochs, ensuring sufficient convergence without overfitting. Gradients are clipped at a maximum norm of 1.0 to prevent exploding gradients. BF16 mixed precision is enabled to reduce memory usage and improve training speed.

B. Experiment Equipment

The proposed experiment is conducted on a lab server running Ubuntu 20.04.6 LTS (Focal Fossa). The system is equipped with a 14th Gen Intel Core i9-14900K processor featuring 24 cores and 32 threads. For graphical computation, the server utilizes an NVIDIA RTX A6000 GPU 48 GB with the proprietary NVIDIA 535.183.01 driver and CUDA 12.2. The system includes 192 GB of RAM and a 4 TB NVMe SSD for primary storage, supplemented by a 14.55 TB external USB drive for dataset storage and backups.

C. Training Result

1) *Training Process*: The training process is monitored using key metrics, including training loss, learning rate, and gradient norm, to ensure effective convergence and robust model performance on unseen data. Fig. 3 presents these metrics: the training loss consistently decreases, indicating effective learning; the learning rate follows a cosine decay schedule for smooth optimization; and the gradient normalization remains controlled, ensuring stable training. During the training process, the loss \mathcal{L} exhibits a rapid decline from approximately 2.0 at the beginning to around 0.6 by 35 steps, after which it stabilizes, indicating convergence. The learning rate η follows a scheduled warm-up and cosine annealing strategy, starting at 3×10^{-5} , warming up to 1×10^{-4} and progressively decreasing to near 0 by 300 steps, aligning with designed learning rate function to enhance model stability. The gradient norm $\|g\|$ shows an initial high value of ~ 2.0 ,

TABLE I: Core metrics for hazard region prediction

Metric	Highway Driving	Urban Driving
BLEU-4 (%)	89.025	88.012
ROUGE-1 (%)	87.313	86.928
ROUGE-2 (%)	72.857	71.957
ROUGE-L (%)	87.324	86.913
MSE (pixels)	42.27	45.56

decreasing over time but exhibiting fluctuations, suggesting adjustments in weight updates during training. This overall trend indicates effective convergence of the model while maintaining controlled parameter updates.

2) *Core Indicators and Performance*: The fine-tuned model’s performance is evaluated using several core indicators, including BLEU-4, ROUGE-L, ROUGE-1, ROUGE-2, and Mean Squared Error (MSE). The BLEU-4 measures the precision of up to 4-gram overlaps between a fine-tuned vision-language model’s generated text and reference outputs, making it useful for tasks like image captioning comparison, ROUGE-1 captures the unigram-level overlap, indicating how well the model covers key information in text summarization tasks, ROUGE-2 extends this to bigrams, offering a finer-grained measure of contextual coverage for summarizing or describing visual content, and ROUGE-L uses the longest common subsequence to evaluate the sequence-level match, emphasizing overall recall of critical information in the model’s output. The fine-tuned model is verified in the highway and urban driving scenarios of the BDD100K human annotation dataset. Each dataset contains 250 frames of driving scenarios, and the *max_samples* is also 250. The model achieved outstanding performance on standard scenarios, as shown in Table I. The model achieved outstanding performance in highway driving scenarios and also great performance in urban driving scenarios. The MSE calculation function is shown below:

$$\text{MSE} = \frac{1}{n} \sum_{i=1}^n ((x_i - x_i^{\text{true}})^2 + (y_i - y_i^{\text{true}})^2) \quad (15)$$

where x_i and y_i represent the prediction from the fine-tuned Qwen2-VL and the x_i^{true} and y_i^{true} represent the human-annotation ground truth pixels location. The model’s qualitative performance is illustrated in Fig. 4, where predicted hazard regions (yellow) closely match the ground truth annotations (red) in most cases. In scenarios involving sudden lane changes or complicated driving scenarios, the model’s performance dropped, as indicated by the higher MSE (3.29 pixels). An example of such a scenario is shown in Fig. 4, where the predicted hazard region slightly deviates from the human-annotated ground truth due to occlusion.

a) *Comparison with Baseline Models*.: As shown in Table II, the proposed LoRA fine-tuned model achieves the highest performance across all reported metrics. Specifically, it obtains an 88.087% BLEU-4 score, far exceeds the next best baseline’s 16.241% (Qwen2-VL-72B), and similarly outperforms other Qwen2-VL variants and Llama3.2-VL-7B by large margins in ROUGE-1, ROUGE-2, and ROUGE-L.

3) *Edge Case Implementation*: The well-fine-tuned Qwen2-VL-7B model proves the capability to analyze and understand

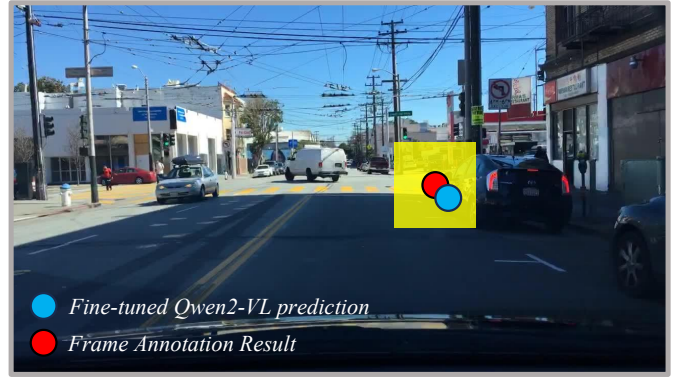


Fig. 4: Comparison of ground truth and predicted coordinates

complex driving scenarios. It can effectively interpret the current scene, taking into account both visual and contextual cues, to provide a comprehensive and accurate understanding of the situation. By using its advanced VLMs’ thought chain, the model identifies potential hazards, highlights key areas of the current frame, and generates actionable insights. Furthermore, it draws attention to specific regions within the environment that require closer observation or immediate action, such as areas with pedestrians, abrupt vehicle movements, or unexpected obstacles. The example implementation is shown in Fig. 5 with the parameter Top-p is 0.9 and Temperature is 0.95.

V. CONCLUSION

This study demonstrates the effectiveness of using fine-tuned VLMs, such as Qwen2-VL, in addressing the challenges of unpredictable edge case scenarios in autonomous driving. By connecting visual and textual modalities, INSIGHT enhances situational edge-case awareness and hazard detection. Experimental results show significant improvements in accuracy for hazard region localization and text generation, outperforming baselines and approaching human-level performance. INSIGHT not only advances the robustness of autonomous systems but also provides a framework for integrating multimodal learning to handle complex and rare driving conditions effectively. Future research could further explore real-time implementations and expand the model’s adaptability to broader datasets, CARLA simulators, and real-world scenarios.



Question Input:
Image Only (None Text)

Answer Output:

The image depicts a clear urban street scene during winter. Key details include:
Traffic Lights: The green light allows vehicles to proceed.
Vehicles: Cars and a white truck are visible, either waiting or moving through the intersection.
Intersection: Busy with vehicles adhering to the traffic signal.
Weather: Clear skies with light snow on the ground, suggesting cold conditions.
Buildings: Residential and commercial structures are visible in the background.
General Scene: A typical winter urban intersection with controlled traffic flow.



Question Input:
In current autonomous driving scenario, which area should we pay more attention on?

Answer Output:

The area around (544,459) should be paid more attention to.



Fig. 5: Demonstration of generalization ability

REFERENCES

- [1] S. Feng, H. Sun, X. Yan, H. Zhu, Z. Zou, S. Shen, and H. X. Liu, "Dense reinforcement learning for safety validation of autonomous vehicles," in *Nature*, 2023.
- [2] L. Chen, P. Wu, K. Chitta, B. Jaeger, A. Geiger, and H. Li, "End-to-end autonomous driving: Challenges and frontiers," in *IEEE Transactions on Pattern Analysis and Machine Intelligence*, 2024.
- [3] M. T. Ribeiro, S. Singh, and C. Guestrin, "why should i trust you?" explaining the predictions of any classifier," in *Proceedings of the 22nd*

ACM SIGKDD international conference on knowledge discovery and data mining, 2016.

- [4] Y. Cui, S. Huang, J. Zhong, Z. Liu, Y. Wang, C. Sun, B. Li, X. Wang, and A. Khajepour, "Drivellm: Charting the path toward full autonomous driving with large language models," in *IEEE Transactions on Intelligent Vehicles*, 2023.
- [5] C. Pan, B. Yaman, T. Nesti, A. Mallik, A. Allievi, S. Velipasalar, and L. Ren, "Vlp: Vision language planning for autonomous driving," in *2024 IEEE/CVF Conference on Computer Vision and Pattern Recognition (CVPR)*, 2024.
- [6] C. Min, D. Zhao, L. Xiao, J. Zhao, X. Xu, Z. Zhu, L. Jin, J. Li, Y. Guo, J. Xing *et al.*, "Driveworld: 4d pre-trained scene understanding via world models for autonomous driving," in *Proceedings of the IEEE/CVF Conference on Computer Vision and Pattern Recognition*, 2024.
- [7] Y. Zhao, L. Wang, X. Yun, C. Chai, Z. Liu, W. Fan, X. Luo, Y. Liu, and X. Qu, "Enhanced scene understanding and situation awareness for autonomous vehicles based on semantic segmentation," in *IEEE Transactions on Systems, Man, and Cybernetics: Systems*, 2024.
- [8] Z. Huang, C. Lv, Y. Xing, and J. Wu, "Multi-modal sensor fusion-based deep neural network for end-to-end autonomous driving with scene understanding," in *IEEE Sensors Journal*, 2020.
- [9] J. Cai, S. Yang, and H. Guang, "A review on scenario generation for testing autonomous vehicles," in *2024 IEEE Intelligent Vehicles Symposium (IV)*, 2024.
- [10] D. Karunakaran, J. S. B. Perez, and S. Worrall, "Generating edge cases for testing autonomous vehicles using real-world data," in *Sensors (Basel, Switzerland)*, 2023.
- [11] Q. Goss, Y. AlRashidi, and M. İ. Akbaş, "Generation of modular and measurable validation scenarios for autonomous vehicles using accident data," in *2021 IEEE Intelligent Vehicles Symposium (IV)*, 2021.
- [12] X. Zhang, J. Tao, K. Tan, M. Törngren, J. M. G. Sánchez, M. R. Ramli, X. Tao, M. Gyllenhammar, F. Wotawa, N. Mohan, M. Nica, and H. Felbinger, "Finding critical scenarios for automated driving systems: A systematic mapping study," in *IEEE Transactions on Software Engineering*, 2023.
- [13] M. Saffary, N. Inampudi, and J. E. Siegel, "Developing a taxonomy of elements adversarial to autonomous vehicles," in *ArXiv*, 2024.
- [14] D. Chen, E. Yurtsever, K. A. Redmill, and Ü. Özgüner, "Using collision momentum in deep reinforcement learning based adversarial pedestrian modeling," in *2023 IEEE Intelligent Vehicles Symposium (IV)*, 2023.
- [15] Y. Luo, M. Meghjani, Q. H. Ho, D. Hsu, and D. Rus, "Interactive planning for autonomous urban driving in adversarial scenarios," in *2021 IEEE International Conference on Robotics and Automation*, 2021.
- [16] D. Chen, Y. Gong, and X. Yang, "Deep reinforcement learning for advanced longitudinal control and collision avoidance in high-risk driving scenarios," in *arXiv*, 2024.
- [17] D. Chen, Y. Gong, and X. T. Yang, "Advanced longitudinal control and collision avoidance for high-risk edge cases in autonomous driving," in *arXiv*, 2025.
- [18] Z. Ghodsi, S. Hari, I. Frosio, T. Tsai, A. J. Troccoli, S. Keckler, S. Garg, and A. Anandkumar, "Generating and characterizing scenarios for safety testing of autonomous vehicles," in *2021 IEEE Intelligent Vehicles Symposium (IV)*, 2021.
- [19] O. Sharma, S. Dash, and M. R. Sial, "A cnn and multi-head attention-based deep learning network for trajectory prediction of autonomous vehicles on multi-lane highways," in *2023 4th IEEE Global Conference for Advancement in Technology (GCAT)*, 2023.
- [20] S. Alsanwy, H. Asadi, M. R. C. Qazani, S. Mohamed, and S. Nahavandi, "A cnn-lstm based model to predict trajectory of human-driven vehicle," in *2023 IEEE International Conference on Systems, Man, and Cybernetics (SMC)*, 2023.
- [21] C. Du, Z. Wang, A. Malcolm, and C. L. Ho, "Imitation learning for autonomous driving based on convolutional and recurrent neural

TABLE II: Core Performance Metrics for Hazard Region Prediction

Metric	Fine-tuned Qwen2-VL-7B	Qwen2-VL-2B	Qwen2-VL-7B	Qwen2-VL-72B	Llama3.2-VL-7B
BLEU-4 (%)	88.087	8.697	14.105	16.241	15.781
ROUGE-1 (%)	87.077	22.308	26.603	28.348	27.824
ROUGE-2 (%)	72.084	7.535	8.022	8.272	8.913
ROUGE-L (%)	87.013	13.875	19.0782	22.713	19.945

- networks,” in *2021 International Conference on High Performance Big Data and Intelligent Systems (HPBD&IS)*, 2021.
- [22] H. P. Rayakota and P.-C. Huang, “Hybridte 2: Hybrid transformer-based end-to-end learning for autonomous driving,” in *2024 IEEE 7th International Conference on Industrial Cyber-Physical Systems*, 2024.
 - [23] D. Chen, N. Wang, F. Chen, and T. Pipe, “Detrive: Imitation learning with transformer detection for end-to-end autonomous driving,” in *arXiv*, 2023.
 - [24] G. Li, Y. Qiu, Y. Yang, Z. Li, S. Li, W. Chu, P. Green, and S. Li, “Lane change strategies for autonomous vehicles: A deep reinforcement learning approach based on transformer,” in *IEEE Transactions on Intelligent Vehicles*, 2023.
 - [25] Z. Zhang, Y. Liu, Z. Peng, M. Chen, D. Xu, and S. Cui, “Digital twin-assisted data-driven optimization for reliable edge caching in wireless networks,” in *IEEE Journal on Selected Areas in Communications*, 2024.
 - [26] K. Renz, L. Chen, A.-M. Marcu, J. Hünemann, B. Hanotte, A. Karnsund, J. Shotton, E. Arani, and O. Sinavski, “Carllava: Vision language models for camera-only closed-loop driving,” in *ArXiv*, 2024.
 - [27] X. Zhou, M. Liu, E. Yurtsever, B. L. Zagar, W. Zimmer, H. Cao, and A. C. Knoll, “Vision language models in autonomous driving: A survey and outlook,” in *IEEE Transactions on Intelligent Vehicles*, 2024.
 - [28] L. Wen, X. Yang, D. Fu, X. Wang, P. Cai, X. Li, T. Ma, Y. Li, L. Xu, D. Shang, Z. Zhu, S. Sun, Y. Bai, X. Cai, M. Dou, S. Hu, B. Shi, and Y. Qiao, “On the road with gpt-4v(ision): Early explorations of visual-language model on autonomous driving,” in *ArXiv*, 2023.
 - [29] P. Zheng, Y. Zhao, Z. Gong, H. Zhu, and S. Wu, “Simplellm4ad: An end-to-end vision-language model with graph visual question answering for autonomous driving,” in *ArXiv*, 2024.
 - [30] Z. Zhang, J. Zhao, C. Huang, and L. Li, “Learning visual semantic map-matching for loosely multi-sensor fusion localization of autonomous vehicles,” in *IEEE Transactions on Intelligent Vehicles*, 2022.
 - [31] Z. Xu, Y. Zhang, E. Xie, Z. Zhao, Y. Guo, K.-Y. K. Wong, Z. Li, and H. Zhao, “Drivegpt4: Interpretable end-to-end autonomous driving via large language model,” in *IEEE Robotics and Automation Letters*, 2024.
 - [32] Z. Wang, R. Shen, and B. Stadie, “Solving robotics problems in zero-shot with vision-language models,” in *arXiv*, 2024.
 - [33] T. Kojima, S. S. Gu, M. Reid, Y. Matsuo, and Y. Iwasawa, “Large language models are zero-shot reasoners,” in *Advances in neural information processing systems*, 2022.
 - [34] J. Rocamonde, V. Montesinos, E. Nava, E. Perez, and D. Lindner, “Vision-language models are zero-shot reward models for reinforcement learning,” in *arXiv*, 2023.
 - [35] J. Wei, Y. Yang, Z. Ma, J. Li, X. Xu, and H. Shen, “Semantic enhanced knowledge graph for large-scale zero-shot learning,” in *ArXiv*, 2022.
 - [36] K. Su, X. Zhang, S. Zhang, J. Zhu, and B. Zhang, “To boost zero-shot generalization for embodied reasoning with vision-language pre-training,” in *IEEE Transactions on Image Processing*, 2024.
 - [37] F. Goudis, K. Papantoniou, K. Papoutsakis, T. Patkos, A. Argyros, and D. Plexousakis, “Fusing domain-specific content from large language models into knowledge graphs for enhanced zero shot object state classification,” in *Proceedings of the AAAI Symposium Series*, 2024.
 - [38] S. J. Reddi, S. Kale, and S. Kumar, “On the convergence of adam and beyond,” *arXiv preprint arXiv:1904.09237*, 2019.
 - [39] P. Wang, S. Bai, S. Tan, S. Wang, Z. Fan, J. Bai, K. Chen, X. Liu, J. Wang, W. Ge *et al.*, “Qwen2-vl: Enhancing vision-language model’s perception of the world at any resolution,” in *arXiv*, 2024.